Nuclear Engineering and Design 398 (2022) 111987

Contents lists available at ScienceDirect

Nuclear Engineering and Design

journal homepage: www.elsevier.com/locate/nucengdes

Effect of contact plasticity on the seismic response of a 7-duct bundle immersed in fluid

Q. Peng [a,b], Y. Jin [a,b], X.P. Su [c], X. Liu [a,b,*], Y.G. Wei [d]

[a] LNM, Institute of Mechanics, Chinese Academy of Sciences, Beijing 100190, China
[b] School of Engineering Science, UCAS, Beijing 100049, China
[c] China Institute of Atomic Energy, Beijing 102413, China
[d] College of Engineering, Peking University, Beijing 100871, China

ARTICLE INFO

Keywords:
Nonlinear contact
Plasticity
Hexagonal bundle
Earthquake
Finite Element Method

ABSTRACT

In the reactor core, the ducts, submerged under fluid, are closely packed. As a result, the collision between ducts is inevitable during the seismic load. Understanding seismic response of the ducts needs to consider both the collision between ducts and the inertial effect from the surrounding fluid. For the collision model, we proposed a nonlinear contact model from a full scale simulation to consider the plastic effect during collision; For the fluid effect, we built an acoustic-structural model to obtain the added mass coefficient depending on the duct's location. Next, we integrated the effects from plastic collision and the fluid inertia into a beam model to study the seismic response of a 7-duct bundle, and then discussed the plastic effect on the contact forces, contact durations and duct acceleration. Results show that although contact plasticity hardly affects the ducts' motion, it has a noticeable effect on both contact force and contact energy dissipation. In addition, our result shows that the contact duration for one typical type of collisions tends to be constant.

1. Introduction

Faster Breeder Reactor (FBR) core, immersed in a liquid coolant, has a hexagonal arrangement of hundreds of ducts (Fujita, 1981). These ducts are maintained by their spikes socketed in a lattice at the bottom of the reactor core. During earthquake, collision between the ducts is inevitable. In order to bear the impact between ducts, the ducts are designed with load pads, also known as spacer pads, at the free end, where the gap between the load pads is usually about several millimeters depending on the design of the reactor core (Bartholf et al., 1989). Therefore, duct collision is a key phenonium to understand the seismic response of the core and has drawn much attention in the past decades (Broc et al., 2019; Catterou et al., 2018; Iwasaki et al., 2017; Kepisty et al., 2017; Koo and Lee, 2007). Moreover, coupled not only by the collision between neighboring ducts, but also by the fluid in-between, duct's seismic response has a much more complex pattern (Peng et al., 2020a).

A few studies have paid attention to the collision between neighboring ducts during earthquake, most of which only focused on the elastic contact. For instance, Sasaki and Muto experimentally studied the seismic responses of a single row of 29 ducts (1:1 scaled) and a matrix of 37 ducts (Sasaki and Muto, 1983). Their experimental results concluded that the collision between the ducts could alter the resonance frequency. In addition, a computer code was also developed, in which fluid effect was considered as added mass and the collision effect was implemented by equivalent spring and damper (Sasaki and Muto, 1983). Using another developed computer code CORALIE (Gauvain and Martelli, 1982), Brochard et al. modeled the impact between ducts by introducing an shock stiffness and a shock damper for a 19-duct scaled mock-up (Brochard et al., 1989). Compared with experiment, their simulation results showed acceptable agreement. Likewise, Horiuchi et al. developed a program SAFA (seismic analysis program for fuel assemblies) to analyze vibration of core component in FBRs (Horiuchi et al., 1995). In their program, collision was modeled with a gap, a linear spring, and a linear damper. Comparison with experimental results confirmed the feasibility of such program.

The gap-spring-damper modeling technique was also adopted in recent years, such as studies by Koo and Lee (Koo and Lee, 2004; Koo and Lee, 2007), by Iwasaki et al. (Iwasaki et al., 2017), and by Broc et al. (Broc and Artini, 2017; Broc et al., 2019; Broc et al., 2015). In these studies, the accuracy of simulation was enhanced by employing such technique. However, contact nonlinearity (contact plasticity for

* Corresponding author at: LNM, Institute of Mechanics, Chinese Academy of Sciences, Beijing 100190, China.
E-mail address: xiaomingliu@imech.ac.cn (X. Liu).

https://doi.org/10.1016/j.nucengdes.2022.111987
Received 13 January 2021; Received in revised form 14 August 2022; Accepted 20 September 2022
Available online 30 September 2022

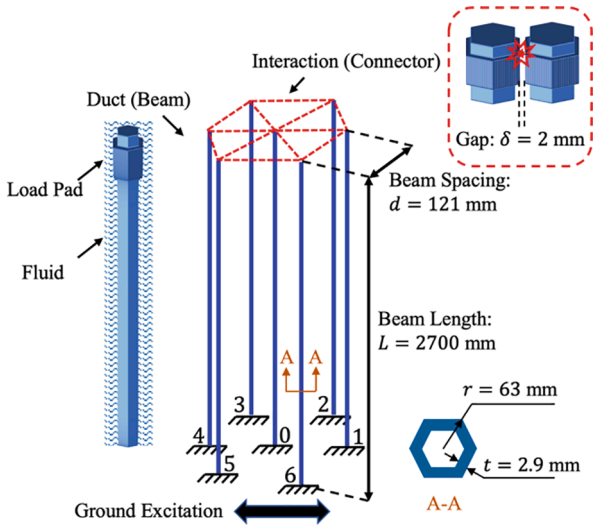

Fig. 1. Finite element beam model. Ducts are abstracted by beams, fluid effect is considered with added mass approach, and interactions (contact) between neighboring ducts are represented by connectors, accounting for gaps, elasticity, plasticity, and damping.

example) was neglected. Under heavy excitation, severe collision between ducts may lead to local plastic deformation, where linear model fails to describe the mechanical behavior (Peng et al., 2020b).

In the present study, we proposed a nonlinear contact model to consider the plastic effect during collision, and then integrated the contact model into a numerical finite element method (FEM) model to study the seismic response of a 7-duct bundle. In addition, fluid effect was considered by applying added mass to each duct depending on its location. Based on this model, we investigated the plastic effect on the contact forces, contact durations and duct acceleration during a typical earthquake. We discovered two types of collision between ducts, one of which is of exactly a half cycle, and the other of which is of the overlap of multiple half cycles. Contact plasticity, predictively occurring under highly intensive seismic excitation, hardly affects the ducts' motion, but has a noticeable effect on both contact force and contact energy dissipation. Thus, the proposed model can also be used to help design the load pads of ducts.

2. Computational method

2.1. Model description

Previous literatures studied the dynamic characteristics of a 7-duct bundle (Nakagawa et al., 1989) and the seismic response (Koo and Lee, 2007). Similarly, in the present work, we studied the seismic response of a 7-duct bundle considering contact plasticity. As shown in Fig. 1, the 7 ducts were arranged in a matrix of hexagonal pattern; the center duct of bundle was labelled 0, and the rest ones were labelled 1 to 6, respectively. The height of the ducts was 2700 mm, the section of the ducts is hexagonal, with a thickness of 2.9 mm and a circumcircle radius of 63 mm. The center-to-center distance between two neighboring ducts was 121 mm. Density of the ducts was 7800 kg/m^3, Youngs modulus and Poisson's ratio were set to 200 GPa and 0.3, respectively. Additional distributed mass was applied over beam length, such that the weight of single beam was 200 kg according to the duct's design. For the material damping, we applied Rayleigh damping with two factors α_R and β_R being 0.6 and 0.0003, respectively (Peng et al., 2020a).

For simulating the earthquake, the seismic excitation was exerted on

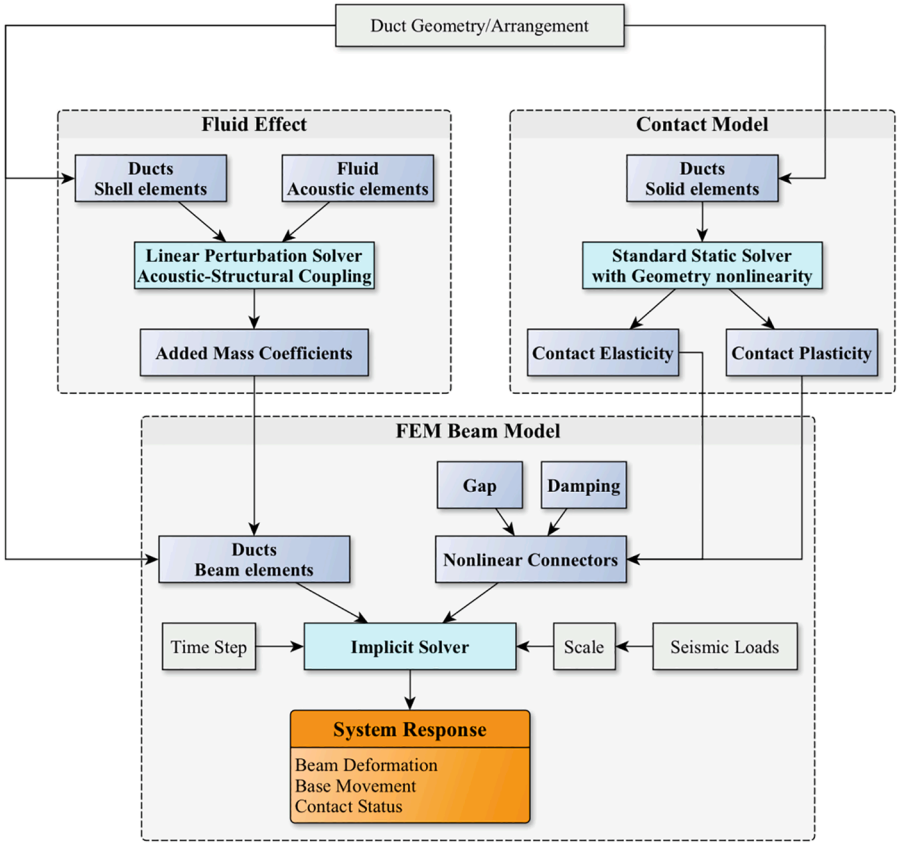

Fig. 2. Computational flow chart. CAS model with linear perturbation solver is adopted to calculate fluid effect and solid model with standard static solver to derive contact law, both of which are fed into FEM beam model as input properties to obtain seismic response.

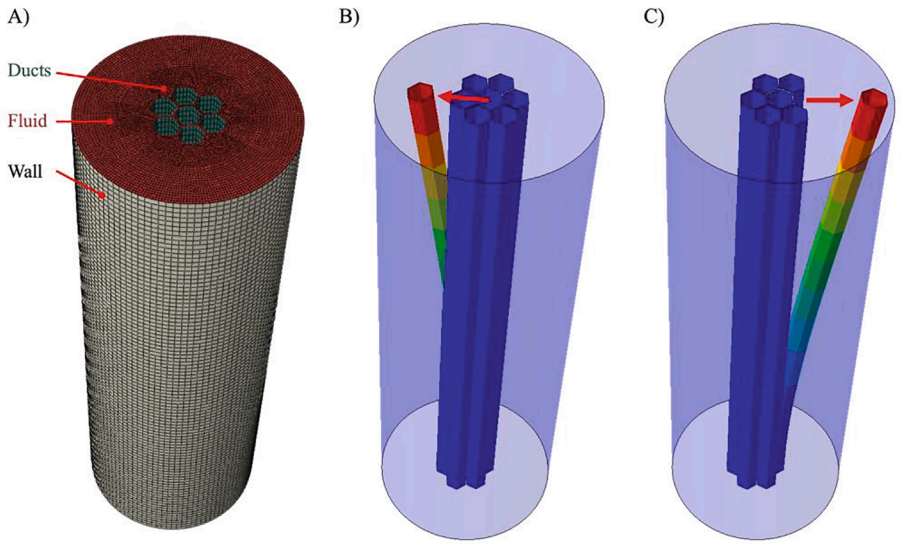

Fig. 3. Coupled acoustic-structural model for determining added mass coefficient. A) Parts and meshes. B) The 1st modal shape for duct 0 with other ducts fixed. C) The 1st modal shape for duct 1 with other ducts fixed.

the bottom of model, as shown in Fig. 1. As in our previous study (Peng et al., 2020a), we selected the same ground excitation, the 1994 Northridge (Newhall – Fire station) record. The peak ground acceleration (PGA) is 0.6 g, 0.6 g, and 0.5 g for *x*-, *y*-, and *z*-direction, respectively. Similar to the scaling method used in literature (Ghaemmaghami and Kianoush, 2010; Pnevmatikos et al., 2020), we scaled the seismic excitation by a factor of 5, 10 and 20 to check the effect of earthquake intensity.

There are two factors which has to be taken into account in the simulation: fluid and collision effect. The first factor is the effect of fluid. Since in a real-world situation, the ducts are immersed under coolant fluid and close packed in a hexagonal pattern, the flow in the gaps of ducts generally coupled with structural deformation and thermal field (Broc and Desbonnets, 2012; Desbonnets and Broc, 2012; Liu and Cheng, 2015). As a computation-effective approach to model the effect of fluid on structural vibration, the method of added mass was commonly adopted (Koo and Lee, 2003; Lu et al., 2018). In the present work, we used added mass to account for different fluid inertia depending on the ducts' location (Fig. 1). Details about fluid effect can be found in Section 2.3.

Second is the collision between ducts. The ducts are closely packed so that the collision is inevitable during the earthquake. During the collision, the initial gap, elastoplastic contact, and damping have to be considered for a reasonable prediction. To model the collision, we used 12 axial nonlinear connectors to associate top nodes of each pair of the neighboring ducts, as shown by the red dashed lines in Fig. 1. Details can be found in Section 2.4.

2.2. Flow chart of the proposed method

Fig. 2 illustrates the flow chart of the computation. In the flow chart, we first proposed two methods to deal with fluid inertia and duct collision, respectively. The fluid inertia on the ducts are obtained by using the coupled acoustic-structural (CAS) model with a linear perturbation solver. The nonlinear collision behavior is obtained by a full-scale finite element simulation of two ducts (solid model) with a standard solver. Following that, the fluid inertia parameters and the collision properties were fed into the FEM beam model to simulate the seismic response. We used 15 beam elements to model each duct, which has enough accuracy for the first three modes of the beam (ABAQUS, 2016; Kepisty et al., 2017; Koo and Lee, 2004; Morishita and Iwata, 1993). The seismic response was computed with an implicit solver with

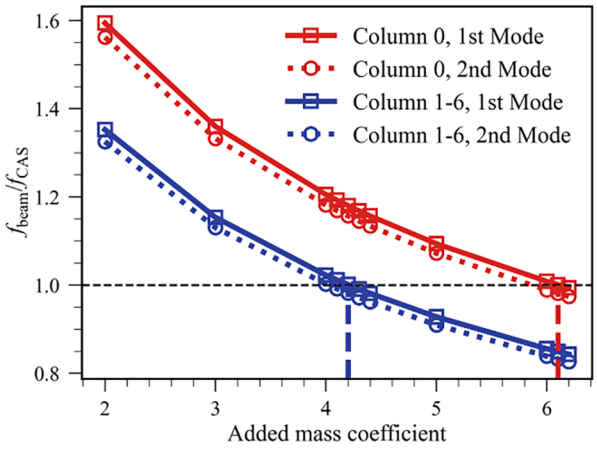

Fig. 4. Determination of added mass coefficient according to CAS model. For center column (column 0), added mass coefficient is set to 6.1, and for peripherical columns (columns 1 – 6), set to 4.2.

Newmark integration, so the integration time step should be selected with discretion. In order to obtain an accurate contact force, the maximum step increment was set to 2e-5 s to make sure that enough data (at least 10 points) was able to be captured during single collision.

2.3. Fluid inertia model

In the FEM beam model, fluid inertia is accounted for by setting added mass for the beams. This type of approach was widely used in the simulation of slender structure immersed under fluid (Li et al., 2018; Liu et al., 2017). It should be noticed that the effect of fluid on the center duct (duct 0) differs from that on the peripherical ducts (ducts 1 – 6). To determine the added mass for each type of duct, a full-scale coupled acoustic-structural model with about 1 million acoustic elements (AC3D8) and 27 thousands shell elements (S4R), as shown in Fig. 3A, was built in our previous study (Peng et al., 2020a), which studied the effects of both the fluid density and the gap width on the eigenfrequencies. In the present study, according to the experiments on the vibration of ducts in which water was used as substitution to liquid metal (Broc et al., 2013; Koo and Lee, 2007; Nakagawa et al., 1989;

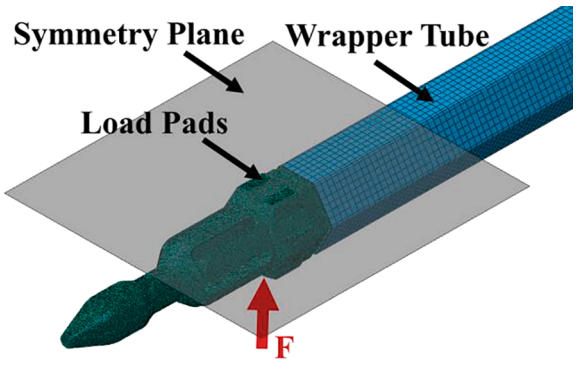

Fig. 5. 3D solid FEM model used to obtain normal force–displacement relationship.

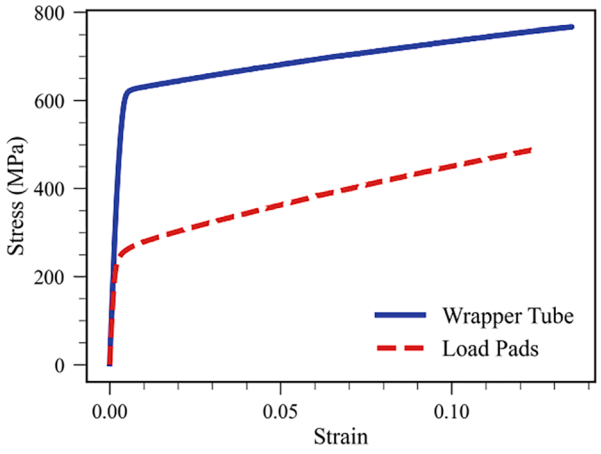

Fig. 6. Materials for 3D solid FEM model: Strain-Stress curve.

Sasaki and Muto, 1983), we also used water as the fluid medium (density was set to 1000 kg/m^3). We set the width of the flow passage between ducts to 6 mm, consistent with our previous study (Peng et al., 2020a). Using linear perturbation solver with Lanczos method, we obtained the 1st and 2nd eigenfrequencies of each duct by fixing all other ducts, respectively.

The coupled acoustic-structural model showed that the 1st and 2nd eigenfrequencies for the center duct 0 were 4.81 Hz and 30.261 Hz respectively; those for the peripherical duct (1 – 6) were 5.67 Hz and 35.666 Hz. Fig. 3B and Fig. 3C shows the 1st modal shapes of duct 0 and duct 1, respectively. These eigenvalues were used as a reference for fluid inertia to build the FEM beam model. In the FEM beam model, according to the beam geometry, we set the section radius to 0.063 m for the fluid inertia. Following that, in order to determine the added mass coefficient for each column, we checked the relationship between the beam frequency and the added mass coefficient, shown in Fig. 4. With such relationship, we could obtain the added mass coefficient for each column by numerically solving $f_{\text{beam}} = f_{\text{CAS}}$, where f_{beam} is the frequency calculated with the beam model and f_{CAS} with the CAS model. As a result, the added mass coefficients for the column 0 and columns 1 – 6 were set to 5.6 and 6.1, respectively.

2.4. Contact force model

Ducts are packed so close that they interact with each other by collisions during earthquake. The load pads of the ducts are designed to bear such impact and prevent reactor catastrophe. However, were the ground excitation extremely intense, plastic deformation would occur.

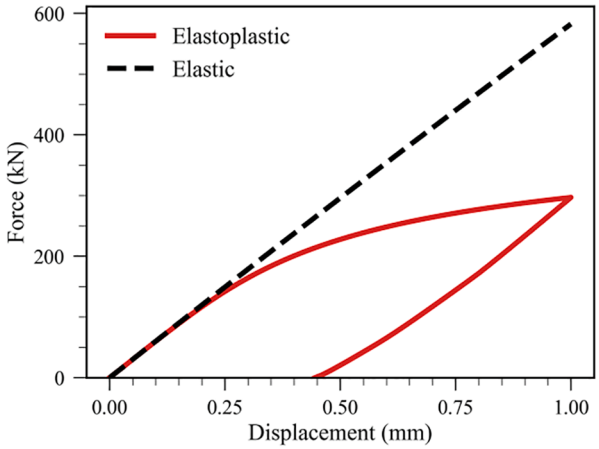

Fig. 7. Normal Force-Displacement curves for contact law that is implemented into FEM beam model as intrinsic properties for axial connectors.

To obtain the contact force model with plasticity, we carried out full scale finite element simulation for the contact between two ducts.

As the system is symmetric, we built a 3D solid FEM model, where the duct was in contact with an analytical rigid plane. The dimension of the duct was 1:1 and the ducts were meshed into about 1.07 million linear elements, a mixture of C3D4 and C3D8R, shown by Fig. 5. The materials for the wrapper tube and load pads are steels. The plasticity of material in the simulation is taken into account by using tensile test data (MTS Landmark 50 kN). The stress-strain curves are shown in Fig. 6. For a comparison between elastic and elastoplastic models, Fig. 7 plots the relationships between the contact force and the compressive displacement for both models. The two models differentiate from each other over 5 % when the contact force is larger than 150 kN, suggesting that elastoplastic model is preferred for intensive excitation. Results show that the elastic contact force is almost linear with the applied displacement, while the plastic contact force shows a highly nonlinear behavior. In the later seismic simulation, these two models were implemented into the FEM beam model by setting nonlinear connector elements between neighboring ducts accordingly.

In the present work, the damping coefficient for the contact is also considered. In order to see the contact damping effect, we varied the damping coefficient from zero to 4800 Ns/m; this value of damping (4800 Ns/m) was used in literature (Kobayashi, 1996). Given all the aforementioned properties, the interaction between beams in the FEM beam model was completely defined.

In sum, we built the present hierarchical model comprising of a coupled acoustic structural model for fluid inertial effect, an elastoplastic model for contact relationship, and a dynamic beam model for the bundle's seismic response. The main assumptions used in the present model are as follows:

1) In the CAS model, the fluid is compressive and inviscid, and linearized surface wave condition is assumed on the free surface of the fluid domain.
2) In the contact model, the elastic and elastoplastic constitutive relationships were assumed for different cases, and the parameters for those relationships were calculated using tensile tests on actual structural material.
3) In the beam model, the interactive between beams can be approximated by a composition of a gap, a nonlinear spring, and a dashpot.

3. Result and discussion

We carried out a full-scale finite element model to obtain the normal force-displacement relationship of the contact, and then used an

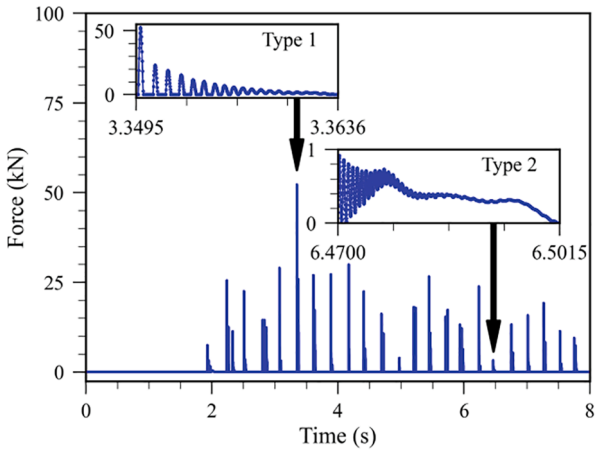

Fig. 8. Contact force between duct 0 and duct 2. Input scale was set to 5 and damping coefficient was set to 4800 Ns/m.

acoustic-structural model to obtain the added mass coefficient for ducts based on their arrangement. Finally, we used a beam model to investigate the seismic response of the ducts under scaled earthquake considering both contact plasticity and fluid effects (models are as in Fig. 1, Fig. 3A, and Fig. 5; computational flow is as in Fig. 2). The results are as follows.

3.1. Two types of collision

During earthquake, collision between ducts appears repeatedly. As an example, Fig. 8 plots the history of contact force between duct 0 and duct 2. With at least 10 points for each collision, the history of contact force had been captured properly. From the figure, there are two types of collisions, one of which is shown in the inset of Fig. 8 beginning at 3.3495 s and the other one of which is shown in the inset beginning at 6.47 s. The former one is of a half cycle (type 1); we defined it as a complete contact. The latter one is of an overlap of many half cycles (type 2); we defined it as a mixed contact, which means this type of contact is mixed with many high frequency contacts and one low frequency contact.

To investigate the relationship of peak contact force and contact duration for each collision, we gathered the peak forces and contact durations for all the collisions (type 1 and type 2). Fig. 9A, Fig. 9B, and Fig. 9C plot the status for all collisions, with abscissa being peak force and ordinate being contact duration. The red dash line in Fig. 9B and Fig. 9C shows that for high ground excitation (scale 10 and 20), contact force will reach the plastic regime, while for low ground excitation (scale 5), the contact is elastic. The distribution of contact duration indicates that, for the type 1 collisions, the contact duration is about 0.3 ms, even under different earthquake intensities; plasticity seems to have little effect on such duration. For the type 2 collisions, the contact duration is usually larger, because this type of contact is always mixed with many high frequency contacts and a low frequency contact. By comparison of Fig. 9A, Fig. 9B, and Fig. 9C, the low frequency contact depends on the intensity of the earthquake: the case with scale 20 has more contacts with longer duration and low contact peak force.

3.2. Effect of contact stiffness on contact duration

In this section, instead of the 7-duct bundle model, we used a simplified FEM beam model to check the effect of contact stiffness on contact duration. Following that, we check the relationship between the contact duration and the fundamental frequency of a corresponding beam/spring analytical model similar to the one used in literature (Catterou et al., 2018). Details are as follows.

The simplified FEM model was composed of two beams: one center beam (column 0) and one peripherical beam (column 1). The section

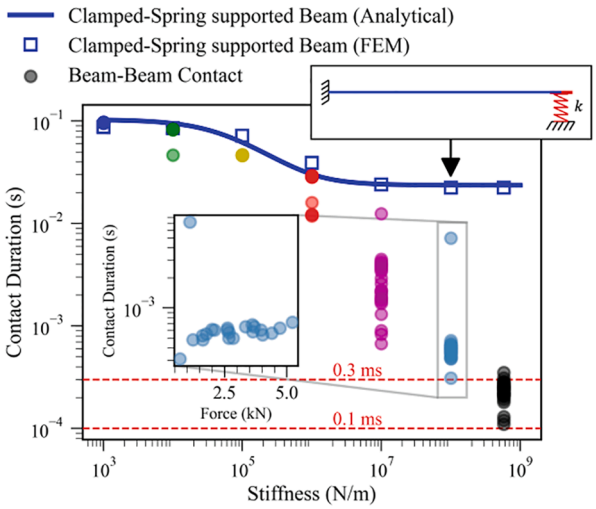

Fig. 10. Contact duration as function of contact stiffness. Inset shows the distribution of contact duration under contact stiffness 10^8 N/m.

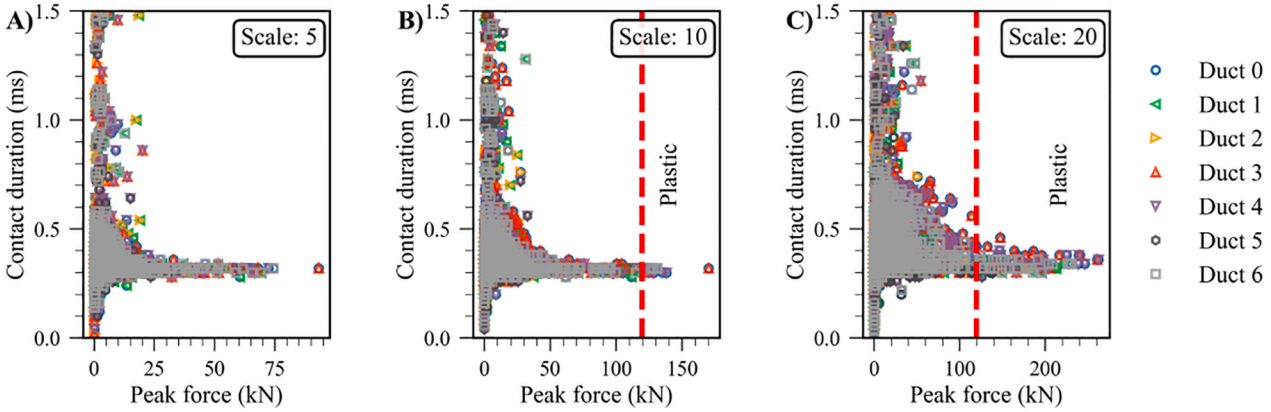

Fig. 9. Scatter plot for collisions under scaled ground excitation: A) scale = 5, B) scale = 10, and C) scale = 20. Every marker represents a single collision, revealing the peak force and contact duration during that collision. The red dash line in B) and C) denotes the peak force reaching plastic regime. (For interpretation of the references to colour in this figure legend, the reader is referred to the web version of this article.)

geometries, meshes, materials were the same as the FEM beam model described in Section 2.1. Instead of using ground excitation, we predefined an initial deflection (6 mm) at the tip of the center beam and then released it to realize the collision between two beams. To model the contact between two beams, we connected two beams with a spring that is compressive only. The stiffness of the spring was set to vary from 1000 N/m to 5.83e8 N/m (same as the elastic contact stiffness in Fig. 7) to study the effect of stiffness on the contact duration. Fig. 10 shows the distribution of contact duration under different contact stiffness. For contact stiffness $k = 5.83e8$ N/m (black dots in Fig. 10), the distribution of contact time is most in the range from 0.1 to 0.3 ms, coherent to the contact duration by the seismic simulation as in Fig. 9. Results also show that, on one hand, overall trend shows that the contact duration decreases with an increasing contact stiffness, although the dispersity may vary. On the other hand, we can find a similar pattern as the one shown in Fig. 9: for a high contact stiffness (larger than 10^7 N/m), the contact duration tends to be a distribution rather than a constant value, but the durations of collisions with high contact force (inset of Fig. 10) tend to converge.

As stated in Section 3.1, the contact between beams is of either single half-cycle or an overlap of multiple half-cycles. The duration of one half-cycle may depend on the fundamental frequency of the beam. To inspect this, we adopted a single-beam model, where one end is clamped and the other end is supported with a spring (Catterou et al., 2018), shown in the inset of Fig. 10. The vibration of the beam can be expressed by.

$$EI\frac{\partial^4 w}{\partial x^4}+\rho A\frac{\partial^2 w}{\partial t^2}=0 \tag{1}$$

with boundary conditions:

$$w|_{x=0}=0$$

$$\left.\frac{\partial w}{\partial x}\right|_{x=0}=0$$

$$\left.EI\frac{\partial^2 w}{\partial x^2}\right|_{x=L}=0$$

$$\left.\left(EI\frac{\partial^3 w}{\partial x^3}-kw\right)\right|_{x=L}=0$$

where w is the deflection of the beam, E the Young's modulus of the beam, I the moment of inertia of the beam, ρ the density of the beam, L the length of the beam, and k the stiffness of the spring. Introducing new dimensionless variables,

$$\hat{x}=\frac{x}{L}$$

$$\hat{w}=\frac{w}{L}$$

$$\hat{t}=t\sqrt{\frac{EI}{\rho AL^4}}$$

we can transform Eq. (1) to the following dimensionless one,

$$\frac{\partial^4 \hat{w}}{\partial \hat{x}^4}+\frac{\partial^2 \hat{w}}{\partial \hat{t}^2}=0 \tag{2}$$

with boundary conditions:

$$\hat{w}|_{\hat{x}=0}=\left.\frac{\partial \hat{w}}{\partial \hat{x}}\right|_{\hat{x}=0}=\left.\frac{\partial^2 \hat{w}}{\partial \hat{x}^2}\right|_{\hat{x}=1}=0 \tag{3}$$

$$\left.\left(\frac{\partial^3 \hat{w}}{\partial \hat{x}^3}-\eta\hat{w}\right)\right|_{\hat{x}=1}=0 \tag{4}$$

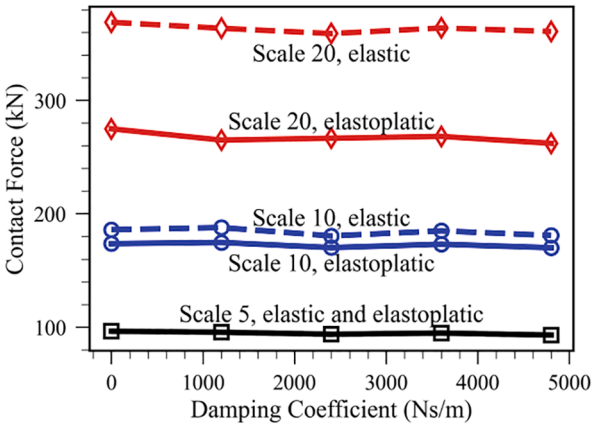

Fig. 11. Maximum contact force under various scales and damping coefficients for elastic and elastoplastic models.

where

$$\eta=\frac{kL^3}{EI}$$

The general solution to Eq. (2) is.

$$\hat{w}=\left(C_1\cos\sqrt{\lambda}\hat{x}+C_2\sin\sqrt{\lambda}\hat{x}+C_3\cosh\sqrt{\lambda}\hat{x}+C_4\sinh\sqrt{\lambda}\hat{x}\right)\left(A\sin\lambda\hat{t}+B\cos\lambda\hat{t}\right) \tag{5}$$

where C_i, A, and B are coefficients to be determined. Substituting Eq. (5) into boundary condition Eq. (3) and (4), we obtain the eigen-equation for λ:

$$\frac{\lambda^{1.5}\left(\cos\sqrt{\lambda}\cosh\sqrt{\lambda}+1\right)}{\cos\sqrt{\lambda}\sinh\sqrt{\lambda}-\sin\sqrt{\lambda}\cosh\sqrt{\lambda}}=\eta \tag{6}$$

For instance, the present duct/spring (inset of Fig. 10) has the following parameters: the stiffness of the spring $k = 5.83e8$ N/m (same as the elastic contact stiffness in Fig. 7), $L = 2.7$ m, $E = 200$ GPa, $A = 1.066e\text{-}3$ m^2, $I = 1.668e\text{-}6$ m^4 and $\rho = 7.9e4$ kg/m^3. Putting all parameters in Eq. (6), we obtain the first root being $\lambda_1 = 15.412$. The corresponding frequency is then $f_1 = \frac{\lambda}{2\pi}\sqrt{\frac{EI}{\rho AL^4}} = 21.176$ Hz.

As in Fig. 10, we varied the contact stiffness k and put it in the Eq. (6). Then, we could derive the half-cycle duration as a function of contact stiffness, shown by the blue solid line in Fig. 10. This relationship was validated with a FEM model (a beam with one end clamped and the other connected with a spring), shown by the blue squares in Fig. 10. By comparing the analytical solution Eq. (6) with the results simulated with the beam-beam contact model (dots in Fig. 10) and the duration by the seismic simulation (dash line in Fig. 10), we found that if we use Eq. (6), the contact duration for $k = 5.83e8$N/m is 23.6 ms, about 77 times larger than the contact duration (0.3 ms) in the seismic simulation (Fig. 9). The reason might be that higher modes are activated by the collision if the contact stiffness is high. Thus, we concluded that the fundamental frequency of a clamped-spring supported beam cannot be used to estimate the contact duration for the case with high contact stiffness.

3.3. Effect of plasticity on contact force

To see how the contact force is affected by the contact damping and earthquake intensity, we plot the peak contact force as a function of the damping coefficient under different intensity of earthquake in Fig. 11. First of all, under low input scale 5, plasticity has little effect on the dynamic response, under medium input scale 10, a slight difference between the elastic and elastoplastic models can be observed, and under

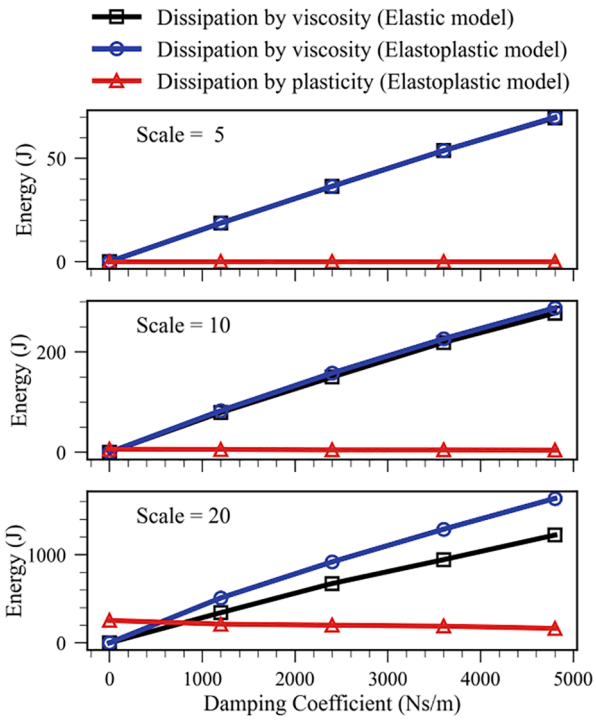

Fig. 12. Energy dissipation by viscosity and plasticity as function of damping coefficient for various scales and models.

large input scale 20, a distinguishable difference is evident. For intensive seismic loads, adopting elastic model can overestimate the contact force and lead to unrealistic results.

We show that local contact force on the load pad may exceed the elastic limit of the material under intensive seismic excitation, and under earthquake, the collisions between ducts occur repeatedly. Recent studies have exhibited that fatigue effect is a key factor for the assessment of the integrity of the fast reactor; the fatigue damage can be originated from local high stress induced by sudden drop of coolant temperature under shutdown condition (Zheng, et al., 2018, Zheng, et al., 2019). Similarly, the cycling contact force can also threaten the integrity of the ducts. In such sense, contact plasticity and contact fatigue should be considered in the design of the load pad. Hence, future investigations on the fatigue effects are required for the safety assessment of the fuel assembly.

It should be point out that by the approach of added mass, although the vibration of beam is well modeled, the mass of beam is also amplified, leading to a possible overestimation of contact impulse. This effect of add mass on the contact dynamics is unknown to date; further investigation is required to make the approach of added mass more accurate.

3.4. Contact energy dissipation during earthquake

Fig. 12 plots the contact energy dissipation as functions of damping coefficient. The energy is dissipated in two ways: dissipation by contact damping and by contact plasticity. For the cases with low input scale 5, deformation is elastic, so the dissipation by plasticity is zero and the dissipations by viscosity are identical for elastic and elastoplastic models. As input scale increases, the energy dissipation by contact plasticity increases. On the other hand, if plastic deformation takes place, the dissipation by viscosity in the elastoplastic model is usually higher than the one in the elastic model. With a given impact speed, plasticity implies lower contact force and thus larger compressive displacement, which in turn accounts for a higher viscosity dissipation (work done by viscosity force). As input scale increases, the difference between the dissipations by contact damping in elastoplastic and elastic models becomes more significant.

It can be concluded that the contribution of energy dissipation by contact plasticity is insignificant for earthquake of low intensity. As for earthquake of high intensity (scale up to 20), the energy dissipation from contact plasticity should be considered, especially when the damping coefficient is less than 1000 Ns/m.

3.5. Motion of ducts during earthquake

Fig. 13 plots the acceleration of the beam tip of duct 0 on *x-y* plane under input scale of 5, 10, and 20 respectively. Under low input scale 5, the scatter points for elastic and elastoplastic models are exactly identical since plastic deformation never occurs. Under medium input scale 10, only a slight difference can be found. In contrast, under large input scale 20, the deviation between these two models becomes more significant, yet most of the scatter points is confined in the same pattern in accordance with the duct's arrangement.

The displacement shows a different trend; the difference in displacement of the duct tip is hardly noticeable, as shown in Fig. 14. Because collision happens occasionally and the contact duration is extremely small compared with overall excitation, the displacement, or equivalently the deflection of beam tip, as a double integration of the acceleration, shows very little difference. Thus, it can be concluded that plasticity has little effect on the duct's displacement, even with high level of earthquake intensity.

4. Conclusion

With FEM beam model incorporated with fluid inertia effect and contact plasticity, we studied the dynamic response of a 7-duct bundle under seismic excitation. Conclusions are listed as follows.

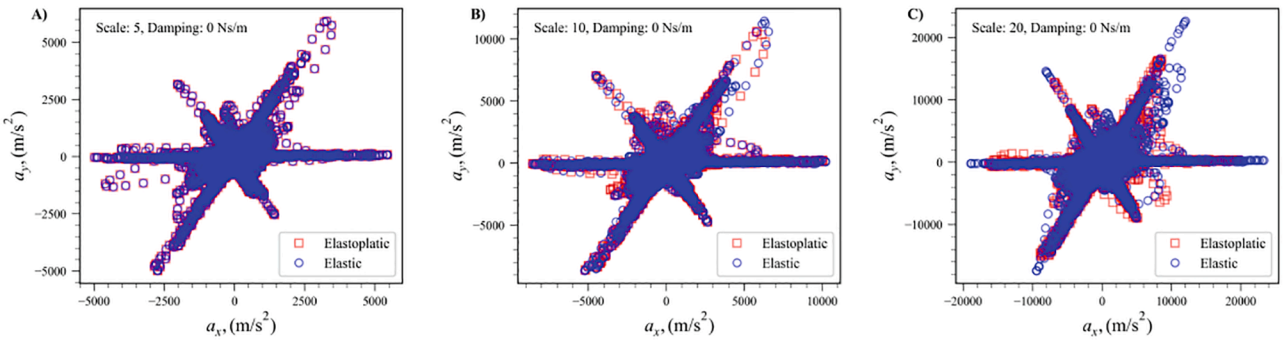

Fig. 13. Scatter plots for the acceleration of the beam tip (duct 0) on *x-y* plane.

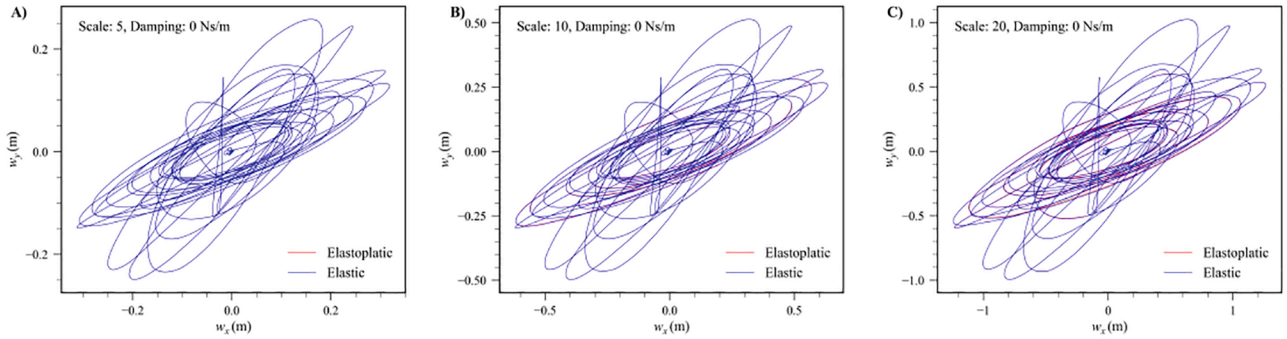

Fig. 14. Deflection trajectories of the beam tip (duct 0) on *x*-*y* plane.

1. The developed model can capture detailed contact about the impact process. There are two types of collisions, one of which is of exactly a half cycle, and the other of which is of the overlap of multiple half cycles. The duration of the type 1 contact tends to be constant, influenced by higher bending modes of the duct if the contact stiffness is high.
2. Ignoring contact plasticity may overestimate the contact peak force and underestimate the energy dissipation by viscosity, and thus leads to unrealistic results.
3. Contact plasticity has effect on the tip acceleration of the ducts in comparison with elastic model, yet its effect on the motion of the beam tip is insignificant.

Declaration of Competing Interest

The authors declare that they have no known competing financial interests or personal relationships that could have appeared to influence the work reported in this paper.

Data availability

No data was used for the research described in the article.

Acknowledgements

This work was supported by the NSFC Basic Science Center Program for “Multiscale Problems in Nonlinear Mechanics” (No.11988102), by the National Natural Science Foundation of China (No. 12022210, 12032001, 11772334), by the Youth Innovation Promotion Association CAS (2018022), and by the Strategic Priority Research Program of the Chinese Academy of Sciences (No. XDB22040501).

References

Abaqus, 2016. ABAQUS Documentation, version 2016. Dassault Systèmes.
Bartholf, L.W., Julyk, L.J., Ryan, J.A., 1989. Vibrational characterization of hexagonal duct core assemblies under various support conditions, International conference on Structural Mechanics in Reactor Technology SMIRT) 10, 9.
Broc, D., Artini, G., 2017. Fluid structure interaction for tubes bundles: presentation of a linear equivalent model. Proceedings of the Asme Pressure Vessels and Piping Conference, 2017, Vol 4, 8.
Broc, D., Desbonnets, Q., 2012. Fluid structure interaction modelling for the vibrartion of tube bundles, part ii: homogenization method based on the navier stokes equations. Proceedings of the Asme Pressure Vessels and Piping Conference (Pvp-2011), Vol 4, 33-40.
Broc, D., Cardolaccia, J., Durand, S., 2013. Dynamic behavior of the Fast Reactor cores: the Symphony program, Fast Reactors and Related Fuel Cycles: Safe Technologies and Sustainable Scenarios (FR13). International Atomic Energy Agency, France.
Broc, D., Cardolaccia, J., Martin, L., Portier, J.L., 2015. Core mechanical dynamics experiment in the phenix reactor. Proceedings of the Asme Pressure Vessels and Piping Conference – 2015, Vol 4, 10.
Broc, D., Artini, G., Cardolaccia, J., Martin, L., 2019. Fast reactor cores seismic excitation in the vertical direction – numerical methods, Proceedings of the ASME Pressure Vessels and Piping Conference – 2018, Vol 8, p. 11.
Brochard, D., Buland, P., Hammami, L., Gantenbein, F., 1989. F.B.R. Core Seismic Analysis, International conference on Structural Mechanics in Reactor Technology (SMIRT) 10, Anaheim, CA, USA.
Catterou, T., Blanc, V., Ricciardi, G., Bourgeois, S., Cochelin, B., 2018. Numerical strategy for dynamic simulation of impacts on SFR fuel pins and experimental validation. Nuclear Engineering and Design 340, 73–85.
Desbonnets, Q., Broc, D., 2012. Fluid structure interaction modelling for the vibration of tube bundles, part i: analysis of the fluid flow in a tube bundle. Proceedings of the Asme Pressure Vessels and Piping Conference (PVP-2011), Vol 4, 25-32.
Fujita, K., 1981. Vibrational characteristics and seismic response analysis of column group in liquid. Bulletin of the Jsme-Japan Society of Mechanical Engineers 24, 1994–2002.
Gauvain, J., Martelli, A., 1982. Numerical integration of the vibratory motion equations of a bundle of flexible beam type structures separated by small gaps, AIMETA, 6° Congresso Nazionale Genova 7-8-9 ottobre.
Ghaemmaghami, A.R., Kianoush, M.R., 2010. Effect of Wall Flexibility on Dynamic Response of Concrete Rectangular Liquid Storage Tanks under Horizontal and Vertical Ground Motions. Journal of Structural Engineering 136, 441–451.
Horiuchi, T., Nakagawa, M., Kasai, H., 1995. Development of SAFA, a seismic analysis program for FBR core components. Nuclear Engineering and Design 157, 37–48.
Iwasaki, A., Matsubara, S., Yamamoto, T., Kitamura, S., Okamura, S., 2017. Core seismic experiment and analysis of a large number of element models for fast reactor. Proceedings of the Asme Pressure Vessels and Piping Conference, 2017, Vol 8, 10.
Kepisty, G., Patricot, C., Broc, D., Campioni, G., 2017. SFR mechanical scenarios and neutron transport transients with CAST3M code. Annals of Nuclear Energy 101, 226–236.
Kobayashi, T., 1996. Evaluation of LMFBR core seismic analysis by the SALCON code, Intercomparison of Liquid Metal Fast Reactor Seismic Analysis Codes Volume 3: Comparison of Observed Effects with Computer Simulated Effects on Reactor Cores from Seismic Disturbances, pp. 113-150.
Koo, G.H., Lee, J.H., 2003. Development of FAMD code to calculate the fluid added mass and damping of arbitrary structures submerged in confined viscous fluid. KSME International Journal 17, 457–466.
Koo, G.H., Lee, J.H., 2004. Fluid effects on the core seismic behavior of a liquid metal reactor. KSME International Journal 18, 2125–2136.
Koo, G.H., Lee, J.H., 2007. An experimental study on LMR core seismic behavior with fluid couplings between closely spaced hexagons. Journal of Mechanical Science and Technology 21, 1008–1017.
Li, W.Z., Lu, D.G., Liu, Y., 2018. Study on the fluid added mass of CAP1400 spent fuel storage rack under vibration condition. Nuclear Engineering and Design 337, 439–449.
Liu, X.J., Cheng, X., 2015. Sub-channel/system coupled code development and its application to SCWR-FQT loop. Nuclear Engineering and Design 285, 39–47.
Liu, Y., Lu, D.G., Li, W.Z., Zhuo, W.Q., 2017. Effect of neighboring wall on the fluid added mass of CAP1400 spent fuel storage rack. Progress in Nuclear Energy 101, 177–187.
Morishita, M., Iwata, K., 1993. Seismic behavior of a freestanding core in a large LMFBR. Nuclear Engineering and Design 140, 309–318.
Nakagawa, M., Horiuchi, T., Kaneto, K., Sawada, S., 1989. Fluid Coupled Effect on Vibration Characteristics of Hexagonal Rod Assemblies, International conference on Structural Mechanics in Reactor Technology (SMIRT) 10. Anaheim, CA, USA.
Peng, Q., Su, X., Li, J., Gao, F., Liu, X., Wei, Y.G., 2020a. Boundary effect on the dynamic response of a 7-hexagon fuel ducts submerged in fluid. Nuclear Engineering and Design 370, 110870.
Peng, Q., Ye, X., Wu, H., Liu, X., Wei, Y.G., 2020b. Effect of plasticity on dynamic impact in a journal-bearing system: A planar case. Mechanism and Machine Theory 154, 104034.
Pnevmatikos, N., Konstandakopoulou, F., Blachowski, B., Papavasileiou, G., Broukos, P. 2020. Multifractal analysis and wavelet leaders for structural damage detection of structures subjected to earthquake excitation. Soil Dynamics and Earthquake Engineering. 139.

Sasaki, Y., Muto, T. 1983. Experimental Studies on Seismic Vibration Phenomena of FBR Core Components, International conference on Structural Mechanics in Reactor Technology (SMIRT) 7, Chicago, USA.

Zheng, S., Lu, D.G., Cao, Q., et al., 2018. Stress and Fatigue Analysis of Thermal Shock for Cladding of Center Measurement Column Lower Head in the Fast Reactor under Shutdown Condition. In: Proceedings of the 26th International Conference on Nuclear Engineering, 2018, vol 6B.

Zheng, S., Lu, D.G., Cao, Q., et al., 2019. Contact model analysis on cladding designs against thermal shock for the lower head of central measuring shroud in a fast reactor. Nuclear Engineering and Design 352, 110204.